13 THE EFFECTS OF AIR TEMPERATURE ON ARCTIC SNOWFALL GAUGE MEASUREMENTS

Rachel E. Jordan*
Jordan Environmental Modeling, PC, Hanover, New Hampshire

Edgar L Andreas
NorthWest Research Associates, Inc., Lebanon, New Hampshire

Konosuke Sugiura
Research Institute for Global Change, Japan Agency for Marine-Earth Science and Technology, Yokosuka, Japan

Daqing Yang
National Hydrology Research Centre, Environment Canada, Saskatoon, Saskatchewan, Canada

1. INTRODUCTION

Measuring snowfall is subject to much more error than measuring rainfall. In polar regions, high winds, cold temperatures, and low precipitation amounts compound this issue; errors of 50 to 100% are not uncommon. Yang et al. (2005), Sugiura et al. (2003), and Bogdanova et al. (2007), among others, discuss the challenges of measuring precipitation under these harsh conditions.

Deflection of snow particles by wind is the major cause of gauge catchment errors. High winds cause smaller and lighter particles to overshoot the orifice; these, thus, do not register as precipitation. Above wind speeds of ~ 6.5 m s^{-1}, snow begins to blow into the gauge; and at still much higher speeds, the problem of wind-induced undercatchment becomes one of overcatchment.

As discussed below, the World Meteorological Organization (WMO) proposed equations to correct for wind-induced undercatchment. Except for wet snow above –2°C, these equations depend primarily on wind speed. Air temperature is not a significant factor. The WMO equations, however, were derived for mid-latitude regions. In this paper, we examine the role that very cold Arctic temperatures have in the correction equations. Because slower growth rates at very low temperatures skew distributions towards smaller particles, we hypothesize increased undercatchment for colder Arctic snow.

*Corresponding author address: Rachel E. Jordan, Jordan Environmental Modeling, PC, 95 E. Wheelock St., Hanover, New Hampshire 03755; e-mail: jim.m.jordan@dartmouth.edu

2. EXTENDING MEASUREMENT STANDARDS TO THE HIGH LATITUDES

From 1986–1998, the WMO oversaw an intercomparison project to examine the errors in solid precipitation measurements by national standard gauges. The WMO adopted the double fence intercomparison reference, or DFIR, as the reference standard. Following accepted procedures, participants worldwide collected precipitation from the most commonly used gauges and from the DFIR.

An important outcome of the WMO study is a set of regression equations for predicting the wind-induced undercatchment or catch ratio (*CR*). *CR*

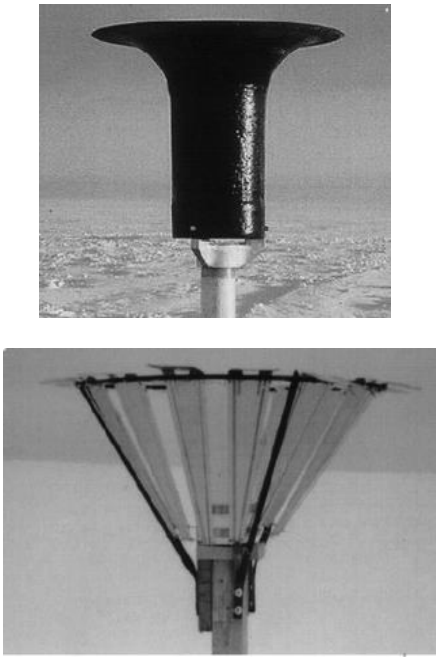

FIG. 1. Canadian Nipher and Russian Tretyakov gauges. (Sugiura et al. 2006,' © Copyright 2006 AMS)

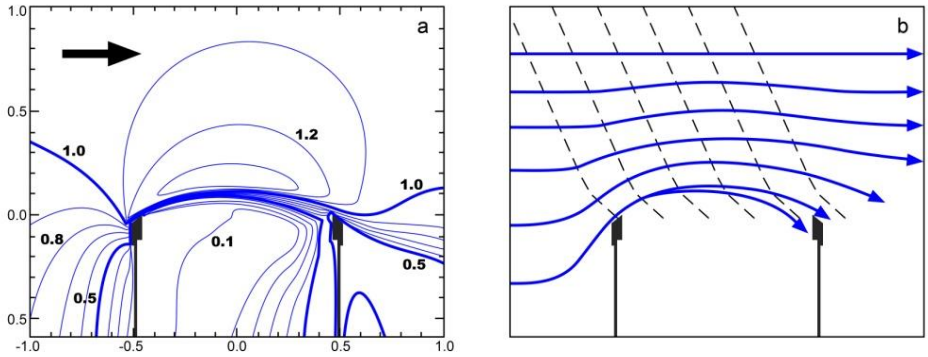

FIG. 2. Mk2 gauge. (a) Normalized contour lines of wind flow (after Nešpor and Sevruk 1999, with modifications, © Copyright 1999 AMS). (b) Schematic wind and snowfall vectors.

computes as the ratio of gauge catch to DFIR catch, after both observations are adjusted for systematic errors, such as wetting and evaporation losses. Since it is an imperfect reference, the DFIR was first corrected to "true" precipitation with the procedures of Yang et al. (1993). For details of the project, see the WMO Final Report (Goodison et al. 1998).

The WMO regression analyses for *CR* excluded precipitation events below 3 mm. Snowfall in the Arctic, however, is often below this threshold, and temperatures are often 15°–20°C colder than in mid-latitudes. To explore the effect of these differences on gauge catch, the Frontier Observational Research System for Global Change and the Water and Environmental Research Center, University of Alaska Fairbanks, extended the WMO intercomparison to high latitudes with a three-year study in Barrow, Alaska (Sugiura et al. 2006, hereafter, SOY06).

We combine the high-latitude Barrow and the mid-latitude WMO datasets to revisit the *CR* regressions for the Canadian Nipher and Russian Tretyakov gauges (Fig. 1). The Barrow study lowered the inclusion threshold from 3 mm to 0.3 mm. As a result, several snowfalls with air temperatures near –30°C are included in our analysis. Because of large scatter in the regressions, we support our hypothesis with theoretical predictions of gauge catch and with simulations of snowfall for "cold" and "warm" atmospheres.

3. THEORETICAL PREDICTIONS OF GAUGE CATCH

Gauges block air flow on their windward sides and accelerate flow over their tops, as shown by the contour lines in Fig. 2a. Because smaller, lighter particles track the flow more closely than do larger, denser particles, uplift at the leading edge of the gauge can cause them to overshoot the orifice (Fig. 2b). For a given wind speed, numerical models first simulate the disturbed flow field about a gauge and then compute particle trajectories within the field. Only gravity and aerodynamic drag act upon the particles. Since fall velocity defines the drag coefficient, wind and fall velocity determine the catch efficiency for a particular gauge.

Particles achieve their terminal velocity when drag and gravitational forces are balanced. Fall velocity (v_t) increases with powers of particle size (D) and of a particle's weight-to-projected-area ratio. Terminal velocity is therefore often expressed as a simple power law. The exponent varies with flow regime, however, and the laws

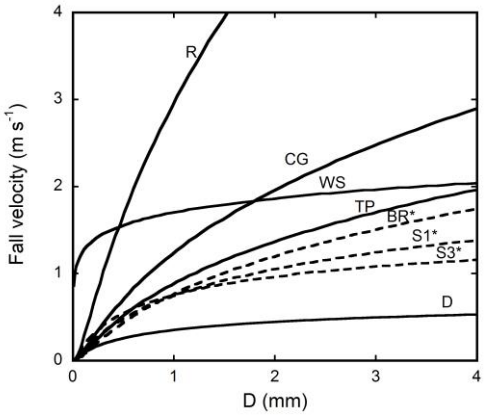

FIG. 3. Fall velocity for selected hydrometeors as functions of particle size, *D*. Wet snow is from Yuter et al. (2006); other habits are computed following Mitchell and Heymsfield (2005). R = rain; CG = cold graupel, WS = wet snow, TP = thick plates, BR* = bullet rosettes, D = dendrites, S1* = side planes; S3* = assemblages of side planes, bullets, and columns. Asterisks and dashes indicate colder particles (< –20°C).

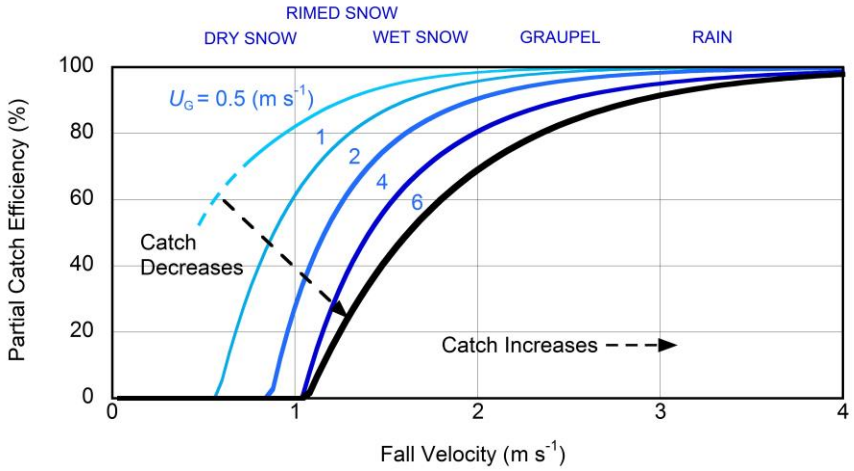

FIG. 4. Numerical catch efficiency of raindrops as a function of fall velocity for the unshielded Hellmann gauge.

apply only within limited size ranges (for details, see Mitchell 1996). For given crystal types, v_t increases with size, as shown in Fig. 3. For given sizes, solid spheres fall the fastest; and open dendrites, the slowest. Wet or rimed particles fall at up to twice the speed of their pristine counterparts.

Nešpor and Sevruk 1999 (hereafter, NS99) use a three-dimensional numerical simulation to compute the trajectories of raindrops within the disturbed flow fields about unshielded Mk2, Hellmann, and ASTA gauges. They subsequently compute the partial catch efficiency or catch ratio (CR_p) as a function of particle diameter and the free wind speed at gauge height (U_G). We combine their parameterization of partial catch efficiency with that for fall velocity to eliminate droplet size and highlight the dependence of CR_p on v_t. Figure 4 shows the variation in CR_p with v_t for the unshielded Hellmann gauge at selected wind speeds. Faster fall speeds increase the catch, while higher wind speeds reduce it.

Using a similar numerical procedure to that for raindrops, Nešpor (1997) computes CR_p for a variety of snow crystal types. The labels across the top of Fig. 4 indicate the mid-ranges of fall velocity for general hydrometeor categories. Although computed for raindrops, the curves approximately apply to snow particles within the appropriate v_t ranges.[1]

Integrating CR_p with the corresponding number density and mass-size relationships yields the integral catch efficiency (or CR) and the mass-weighted fall velocity. Thériault et al. (2012) use a procedure similar to NS99 to simulate the catch ratio of an Alter-shielded Geonor gauge for various snow habits. Figure 5 shows their computations for "dry" snow and graupel. Wind shields slow wind speed across the orifice and can double or triple the catch of unshielded gauges.

[1]Nešpor (1997), for instance, simulates CR_p = 95% and 20% for 4-mm dendrites at U_G = 0.5 and 1 m s^{-1}; and CR_p = 98% and 57% at U_G = 0.5 and 3 m s^{-1} for 2-mm cold graupel.

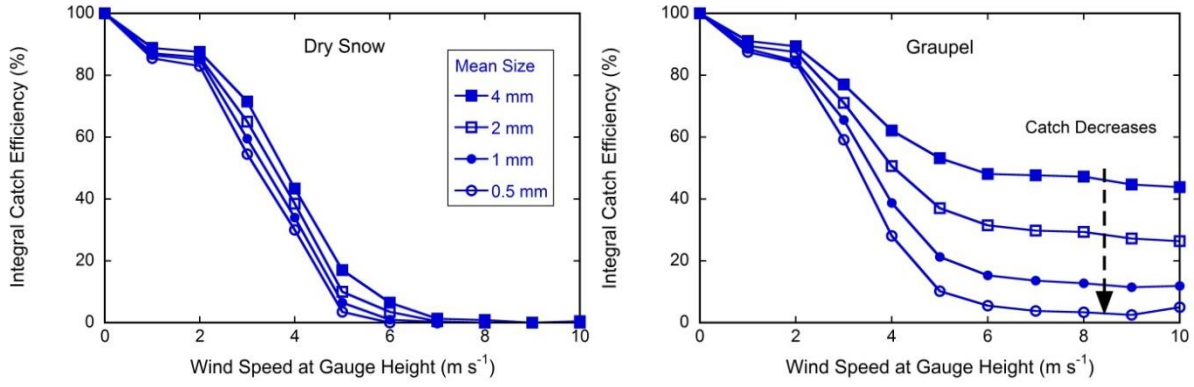

FIG. 5. Variation of the integral catch efficiency (or catch ratio) with wind speed for selected mean sizes. "Dry" snow consists of dendrites and radiating assemblages of plates. (After Thériault et al. 2012, © Copyright 2012 AMS).

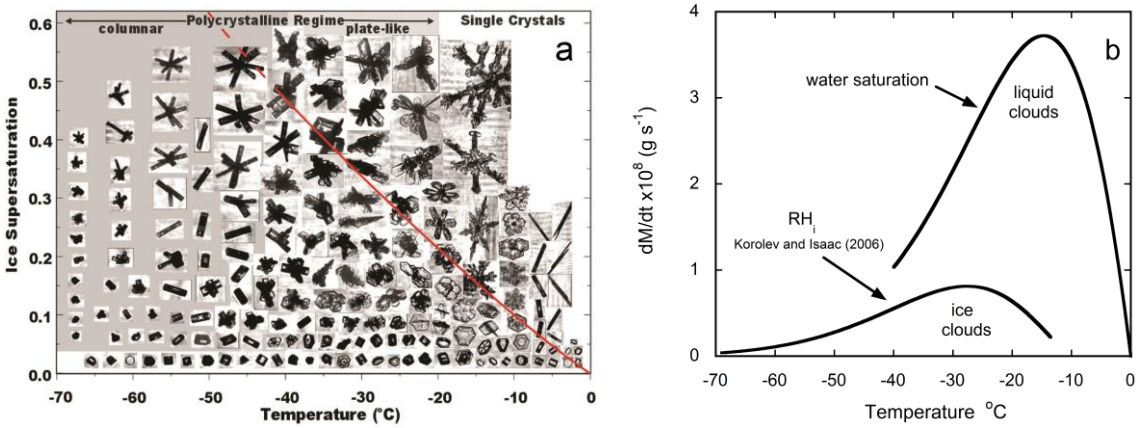

FIG. 6. (a) Pictorial habit diagram of Bailey and Hallett (2009) based on laboratory and flight imagery (© Copyright 2009 AMS). The red line indicates water saturation. (b) Diffusional growth rate of an ice crystal with $C = 1/4\pi$ in liquid and ice clouds at respective pressure levels of 850 and 650 hPa [eq. 13-76, Pruppacher and Klett (1997)].

4. RELATING FALL VELOCITY TO TEMPERATURE

The numerical studies of Nešpor (1997) and Thériault et al. (2012) provide convincing evidence that *CR* decreases with wind speed and increases with fall velocity. Connecting fall velocity with near-surface temperature, however, is rather indirect.

Temperature impacts crystal growth both by controlling the habit (and hence the weight-to-projected-area ratio) and by setting limits on the vapor pressure. Variations in crystal habit are the most extreme at the warm end of the habit diagram (Fig. 6a). In their observations of crystal growth in vertical cloud tunnels, Takahashi et al. (1991) measured more-or-less oscillatory variations in fall velocity with temperature between −3° and −23°C. Minima in fall velocities occur for needles and dendrites and maxima for isometric thick plates at −9.2° and −19.0°C. Isometric particles begin to rime after 10 to 20 minutes of growth and eventually turn into graupel.

We are unaware of similar observations for colder particles but speculate that particle size rather than habit plays the dominant role in this regime, where the growth rate drops off steeply (Fig. 6b). The proximity of the fall velocity curves for the three cold habits in Fig. 3 concurs with this assumption. Phase as well as temperature determines the excess vapor available for particle growth. Figure 6b shows the diffusional growth rates of a crystal with a capacitance (C) of $1/4\pi$ in liquid and ice clouds at pressure levels of 850 and 650 hPa. The former assumes water saturation; the latter uses Korolev and Isaac's (2006) empirical function, which predicts supersaturation that is about mid-way between water and ice saturation. Ice, mixed-phase, and liquid clouds are present throughout the year in the Arctic, with the amount of liquid increasing at lower levels and during the summer (Shupe 2011). No liquid exists below −40°C and no pure ice clouds exist above ~ −13°C.

In the absence of strong convection, which is mostly the case in Arctic winters (Morrison et al. 2003), the growth rate is generally bounded by the two curves in Fig. 6b and therefore increases with temperature below ~ −15°C. The average temperature at gauge-height (T_G) during winter precipitation events at Barrow was ~ −21°C. Even if there were a 10°C temperature inversion at the surface, most crystal growth should occur within this colder regime. Despite uncertainty, we argue that a weak correlation exits between v_t and T_G. In addition to reduced diffusional growth, the prevalence of diamond dust during the coldest months (Intrieri and Shupe 2004) and the increased likelihood of riming and aggregation at warmer temperatures support our case.

5. MODELING THE EVOLUTION OF FALL VELOCITY AND SNOWFALL

We use the Snow Growth Model (hereafter, SGM; Mitchell et al. 2006) to simulate the vertical evolution of fall velocity and snowfall in "cold" and "warm" cloud examples from the SHEBA (Surface Heat Budget of the Arctic Ocean) experiment. The SGM predicts the evolution of snow particle spectra through processes of deposition and aggregation. It assumes a gamma particle size distribution:

$$N(D) = N_0 D^{\mu} \exp^{-\Lambda D} \qquad (1)$$

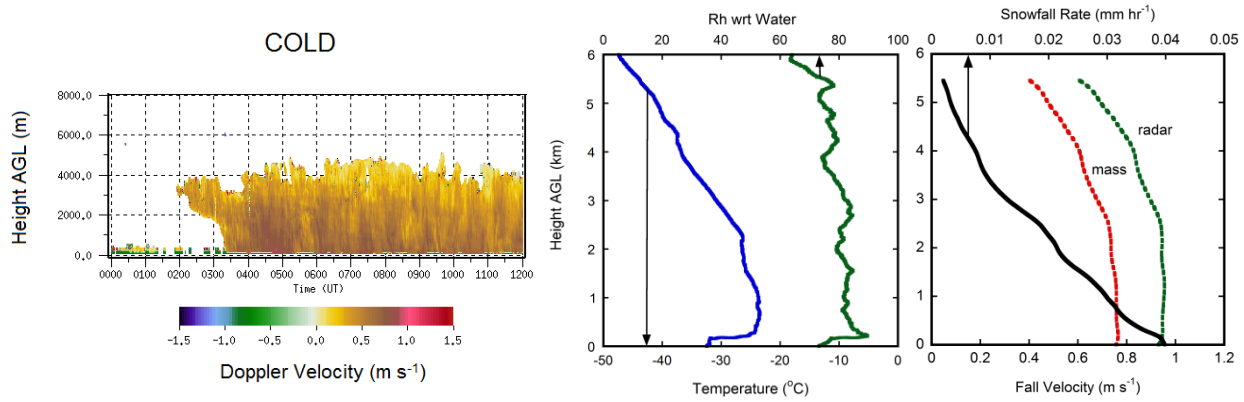

FIG. 7. Left) MMCR Doppler velocity from SHEBA for 21 Dec 1997, Middle) Radiosonde observations of air temperature and relative humidity from SHEBA (1113 hrs), and Right) SGM simulations of snowfall rate (solid line), mass- and radar-weighted fall velocity (dotted lines).

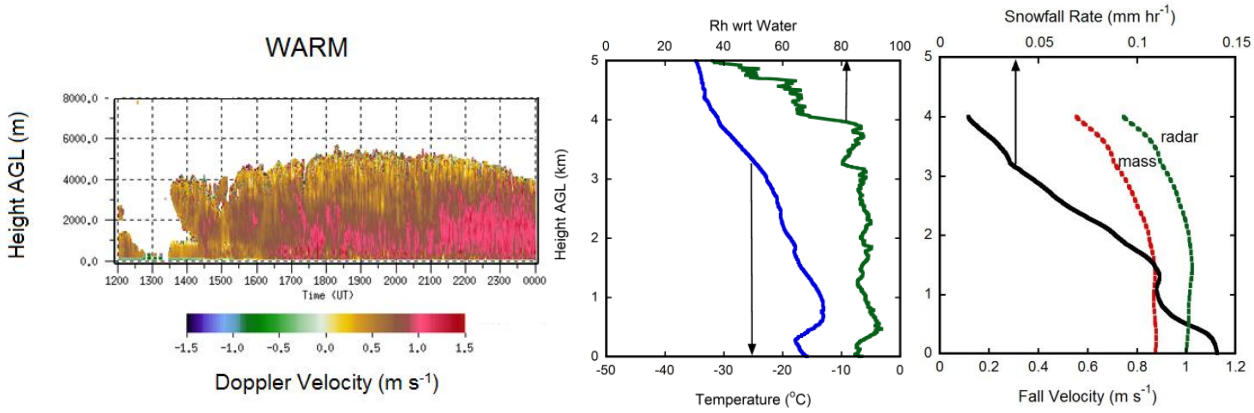

FIG. 8. As in Fig. 7 but for 5 Nov 1997. Radiosonde launch on 6 Nov at 0000 hrs.

with a dispersion, μ, of -0.6. Coupled 0th and 2nd mass moments solve for the slope, Λ, and particle number concentration, N, of the particle size distribution at descending levels through the cloud. Here, N is the integral of eq. (1): $N = N_0\Gamma(1+\mu)/\Lambda^{1+\mu}$ and N_0 is the distribution intercept. For this application, we modified the SGM to use coupled 0th and 1st mass moments, rather than the mass-squared or radar moment.

The left and middle panels in Figs. 7 and 8 show millimeter-wavelength cloud radar (MMCR) images of Doppler velocity and radiosonde data from SHEBA. The right panel shows modeled snowfall rate and fall velocity (mass- and radar-weighted) computed from the radiosonde temperature and humidity profiles. At this stage, the SGM does not treat nucleation and sets the updraft velocity to 0. N at cloud top was therefore initialized with companion MMCR images of Doppler reflectivity and with an empirical function (Ryan, 1996) which relates mean particle size to temperature.

In selecting the two examples, we sought mid-level, stratiform clouds with near-surface temperatures below –15°C and without significant blowing snow. These proved hard to find since heavier winter storms at SHEBA were often accompanied by high winds. In addition, many warmer storms had significant sub-cloud evaporation, as evidenced in both the radar imagery and radiosonde data.

For the cold case, relative humidity with respect to ice (RH_i) was between 119 and 111% in the upper part of the cloud. In conformance with the habit diagram (Fig. 6a), we chose "assemblages of side planes, columns and bullets (S3)" as the crystal type. Growth rates were close to those for ice clouds at the same temperature and pressure. The SGM predicted a snowfall rate of 0.040 mm hr^{-1} and a mass-weighted fall velocity of 0.76 m s^{-1} at the surface.

.

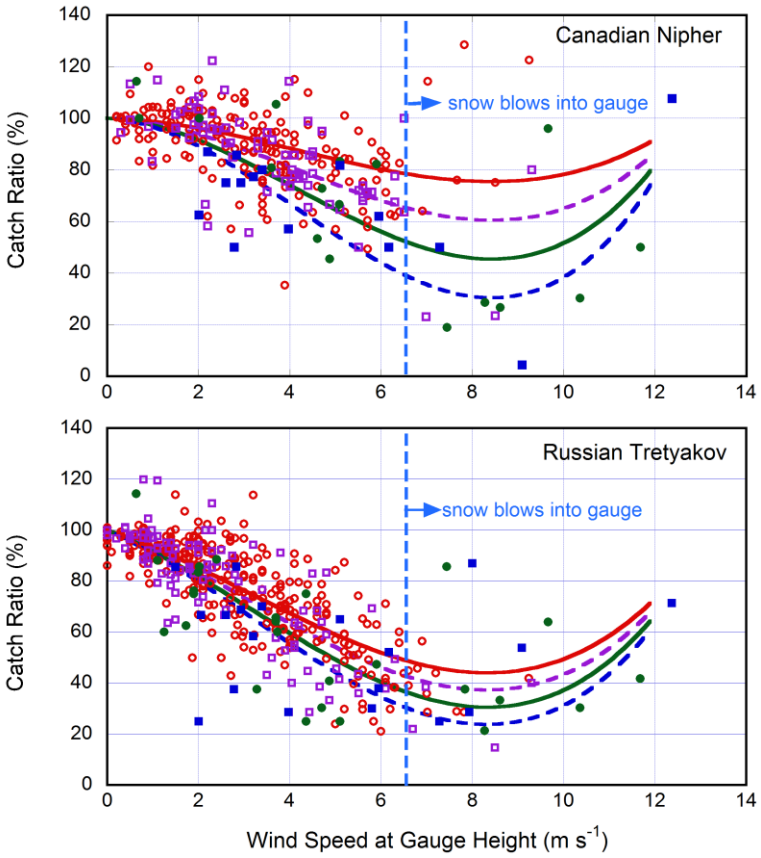

FIG. 9. Data from the combined WMO and Barrow datasets:
○: ≥ –8.0°C, □: –8.0°C to –16.0°C, ●: –16.0°C to –24.0°C, ■: ≤ –24.0°C
Curves computed from (2): —— 0.0°C, - - - –10.0°C, —— –20.0°C, - - - –30.0°C

For the warm case, RH_i was slightly lower than for the cold case, but higher than for comparable ice clouds. Growth rates were consequently also higher. We chose Mitchell's "generic snow" as a crystal type. The SGM predicted a snowfall rate of 0.140 mm hr^{-1} and a mass-weighted fall velocity of 0.88 m s^{-1} at the surface. Simulated velocities were therefore about 16% faster for the warm case, even though the assumed cloud thickness was less. The SHEBA Project Office (SPO) measured snowfall with the Canadian Nipher gauge and applied the WMO procedures to correct the data.[2] In both simulations, snowfall rates were in line with these observations.

6. REGRESSION RESULTS AND DISCUSSION

Theory predicts a 100% gauge catch in calm conditions, independent of the fall velocity. In fitting the regressions, we therefore choose the following functional relationship for *CR*:

$$CR(\%) = 100 + \left(aU_G + bU_G^2 + cU_G^3\right)\left(1 + a1\,T_G\right) \quad \text{for } U_G < 12 \text{ m s}^{-1} \qquad (2)$$

Using the combined WMO (Goodison et al. 1998) and Barrow (SOY06) data sets, we regressed *CR* against U_G and T_G to obtain the coefficients in (2).[3] Figure 9 shows the results for

[2] See the website http://www.eol.ucar.edu/projects/sheba/; Author/PI Moritz, R.; Ice Camp Daily Precipitation Amount.

[3] Canadian Nipher:
a = –.2734, *b* = –0.9715, *c* = 0.0782, *a1* = –0.0613
Russian Tretyakov:
a = –5.7436, *b* = –1.0456, *c* = 0.1114, *a1* = –0.0121

selected temperatures. Despite large scatter, both regressions capture the decrease in catch with smaller sizes/lower temperatures as predicted by theory (Fig. 5). The improvement in r-square with the addition of temperature was significant for the Nipher gauge (0.32 to 0.42) but quite modest for the Tretyakov gauge (0.63 to 0.65). We did not attempt to optimize the exponents in the U_G polynomial or on T_G, which could have produced closer fits.

The regression equations also show a reduction in undercatchment with the onset of blowing snow at around U_G = 6.5 m s^{-1}. Since the WMO data were limited to $U_G \leq 8.0$ m s^{-1}, only the Barrow data reflect this trend.

From October through March at SHEBA, almost 60% of recorded precipitation events were below the 0.3 mm threshold set by SOY06. Many of the coldest snowfalls occurred as trace amounts. While inclusion of these events could lend support to our hypothesis, it is not possible to determine the catch ratio of such small quantities.

Matrosov et al. (2008) compared snowfall retrievals from radar at SHEBA with the SPO-corrected measurements for ten selected storms. We used eq. (2) to correct the same data. Our results were generally closer to the radar retrievals and higher than the SPO values (with the exception of a blowing snow event, which was lower than the SPO corrected value). This concurs with the assertion of Sturm et al. (2002) that the recorded SHEBA measurements were biased low.

7. CONCLUSIONS

After having run simulations for several SHEBA snowfalls (in addition to those shown here), we conclude that a weak relationship exists between the mass-weighted fall speed and near-surface temperature and that gauge catch, overall, is likely lower for cold Arctic conditions. The unexpected factor working against our hypothesis was sub-cloud evaporation during the warmer snowfalls at SHEBA. Further investigation is required to determine if this was a real factor or, perhaps, a dry bias in the radiosonde data. Given these and other uncertainties, we regard the coefficients in the regression equations as preliminary.

Besides temperature, precipitation amount may play a role in determining wind-induced undercatchment. NS99 (their Fig. 12) and SOY06 (their Fig. 13) both observed that catch ratio correlates with precipitation rate. Because mass-weighted fall velocity is a function of the distribution slope (Λ) and because precipitation rate is a function of Λ and particle number concentration (*N)*, this relationship has a sound theoretical basis. The difficulty is in knowing *N*. For rain, its impact is indirectly parameterized by the type of storm. Such relationships have not been worked out for cold snow. Investigating cloud properties in the Arctic by means of over-flights (e.g., Morrison et al. 2011) and ground-based radar retrievals should shed light on the relationship between *N* and the snowfall rate.

A definitive test of the effect of fall velocity on gauge catch could be achieved by simultaneous measurements of wind undercatchment and Doppler velocity and reflectivity.

8. ACKNOWLEDGMENTS

The US National Science Foundation supported this work through award ARC-1019322. We express our gratitude to the many WMO contributors and to the NOAA/CMDL staff and the Barrow Arctic Science Consortium for collecting the precipitation data. We thank David Mitchell for providing his Snow Growth Model, Vladislav Neŝpor for providing additional material on snowfall undercatchment, Janet Intrieri for help with interpreting the SHEBA radar imagery, Taneil Uttal for the NOAA/ESRL radar velocity images, Richard Moritz for the NCAR/GLAS radiosonde data and the SPO precipitation data, and Barry Goodison for his helpful comments. We also thank Emily Moynihan of BlytheVisual. LLC, for the poster preparation.

9. REFERENCES

Bailey, M. P., and J. Hallett, 2009: A comprehensive habit diagram for atmospheric ice crystals: Confirmation from the laboratory, AIRS II, and other field studies. *J. Atmos. Sci*., **66**, 2888–2899.

Bogdanova, E. G., B. M. Il'in, and S. Yu. Gavrilova, 2007: Advanced methods for correcting measured precipitation and results of their application in the polar regions of Russia and North America. *Russ. Meteor. Hydrol*., **32**, 229–244.

Goodison, B. E., P. Y. T. Louie, and D. Yang, 1998: WMO solid precipitation measurement intercomparison final report. WMO/Tech. Doc. 872, World Meteorological Organization, Geneva, 212 pp.

Intrieri, J. M., and M. D. Shupe, 2004: Characteristics and radiative effects of diamond dust over the western Arctic Ocean region. *J. Climate*, **17**, 2953–2960.

Korolev, A., and G. A. Isaac, 2006: Relative humidity in liquid, mixed-phase, and ice clouds. *J. Atmos. Sci*., **63**, 2865–2880.

Matrosov, S. Y., M. D. Shupe, and I. V. Djalalova, 2008: Snowfall retrievals using millimeter-wavelength cloud radars. *J. Appl. Meteor. Climatol*., **47**, 769–777.

Mitchell, D. L., 1996: Use of mass- and area-dimensional power laws for determining precipitation particle terminal velocities. *J. Atmos. Sci.*, **53**, 1710–1723.

Mitchell, D. L., and A. J. Heymsfield, 2005: Refinements in the treatment of ice particle terminal velocities, highlighting aggregates. *J. Atmos. Sci.*, **62**, 1637–1644.

Mitchell, D. L., A. Huggins, and V. Grubisic, 2006: A new snow growth model with application to radar precipitation estimates. *Atmos. Res*., **82**, 2–18.

Morrison, H, M. D. Shupe, and J. A. Curry, 2003: Modeling clouds observed at SHEBA using a bulk microphysics parameterization implemented into a single-column model. *J. Geophys. Res.*, **108** (D8), doi:10.1029/2002JD00229.

Morrison, H, P. Zuidema, G. M. McFarquhar, A. Bansemer, and A. J. Heymsfield, 2011: Snow microphysical observations in shallow mixed-phase and deep frontal Arctic cloud systems, *Quart. J. Roy. Meteor. Soc.*, **137**, 1589 – 1601.

Nešpor, V., 1997: Investigation of wind-induced error of rain and snow measurements using numerical simulation. 25 pp. [Available from the author, Department of Geography, Swiss Federal Institute of Technology (ETH), Winterthurerstr. 190, 8057 Zurich, Switzerland, email: nespor@geo.umnw.ethz.ch]

Nešpor, V., and B. Sevruk, 1999: Estimation of wind-induced error of rainfall gauge measurements using a numerical simulation. *J. Atmos. Oceanic Technol*., **16**, 450–464.

Pruppacher, H. R., and J. D. Klett, 1997: *Microphysics of Clouds and Precipitation*. 2nd ed. Kluwer Academic Publishers, 954 pp.

Ryan, B. F., 1996: On the global variation of precipitating layer clouds. *Bull. Amer. Meteor. Soc.*, **77**, 53–70.

Shupe, M. D., 2011: Clouds at Arctic atmospheric observatories. Part II: Thermodynamic phase characteristics. *J. Appl. Meteor. Climatol*., **50**, 645–660.

Sturm, M., J. Holmgren, and D. K. Perovich, 2002: Winter snow cover on the sea ice of the Arctic Ocean at the Surface Heat Budget of the Arctic Ocean (SHEBA): Temporal evolution and spatial variability. *J. Geophys. Res.*, **107** (C10), doi:10.1029/2000JC000400.

Sugiura, K., D. Yang, and T. Ohata, 2003: Systematic error aspects of gauge-measured solid precipitation in the Arctic, Barrow, Alaska. *Geophys. Res. Lett.*, **30**, 1192, doi:10.1029/2002GL015547.

Sugiura, K., T. Ohata, and D. Yang, 2006: Catch characteristics of precipitation in high-latitude regions with high winds. *J. Hydrometeor*., **7**, 984–994.

Takahashi, T., T. Endoh, G. Wakahama, and N. Fukuta, 1991: Vapor diffusional growth of free-falling snow crystals, *J. Meteor. Soc. Japan*, **69**, 15–30.

Thériault, J. M., R. Rasmussen, K. Ikeda, and S. Landolt, 2012: Dependence of snow gauge collection efficiency on snowflake characteristics. *J. Appl. Meteor. Climatol*., **51**, 745–762.

Yang, D., J. R. Metcalfe, B. E. Goodison, and E. Mekis, 1993: An evaluation of the double fence intercomparison reference gauge. *Proc. Eastern Snow Conf., 50th Meeting,* Quebec City, Canada, Eastern Snow Conference, 105–111.

Yang, D., D. Kane, Z. Zhang, D. Legates, and B. Goodison, 2005: Bias corrections of long-term (1973–2004) daily precipitation data over the northern regions. *Geophys. Res. Lett.*, **32**, L19501, doi:10.1029/2005GL024057.

Yuter, S., D. E. Kingsmill, L. B. Nance, and M. Lőffler-Mang, 2006: Observations of precipitation size and fall speed characteristics within coexisting rain and wet snow. *J. Appl. Meteor. Climatol*., **45**, 1450–1464.